Modeling and spectroscopic studies of bisphosphonate–bone interactions. The Raman, NMR and crystallographic investigations of Ca–HEDP complexes

Ignacy Cukrowski[a],*, Ljiljana,Popović[a], Werner Barnard[a], Sylvia O. Paul[b], Petrus H. van Rooyen[a,*], David C. Liles[a]

[a]Department of Chemistry, University of Pretoria, Pretoria, 0002, South Africa
[b]Department of Chemistry, University of South Africa, Pretoria, PO Box 392, 0003, South Africa

*Corresponding authors. I. Cukrowski is to be contacted at fax: +27 12 362 5297. P.H. van Rooyen, fax: +27 12 362 5297. Emails: ignacy.cukrowski@up.ac.za; phvr@up.ac.za

Abstract

Raman spectroscopy was used to study the interactions of bovine bone, hydroxyapatite (HA, as a model of bone) and calcium hydrogen phosphate ($CaHPO_4$) with 1-hydroxyethylidene-1,1-diphosphonic acid, $CH_3C(OH)(PO_3H_2)_2$ (HEDP, the oldest known member in the class of bisphosphonates (BPs) that is commonly used as (i) a reference compound for BP activity, a scale of a BP's potency, and (ii) a pain palliative agent). Raman spectra with diminished background fluorescence were obtained using a visible laser line of 514.5 nm. The Raman spectra of the products from the reaction of HEDP with bone, HA and $CaHPO_4$ could be considered virtually identical. This strongly suggests that $CaHPO_4$ forms first from the reaction of bone or HA with HEDP (which also acts as a strong acid), upon which free Ca^{2+} ions become available for complexation reactions with HEDP. Two complexes were observed using Raman spectroscopy for each of the interactions of HEDP studied here. This shows that HA can be substituted for bone in studies concerned with the interaction of bone with chemical compounds. Also, Raman spectroscopy can be utilized to distinguish between different complexes formed at the solid/solution interface. One of the two complexes has been further characterized using Nuclear Magnetic Resonance (NMR) spectroscopy, as well as single crystal and powder X-ray diffraction (XRD). This complex has been found to be calcium dihydrogen ethane-1-hydroxy-1,1-diphosphonate dihydrate ($Ca(CH_3C(OH)(PO_3H)_2)\cdot 2H_2O$). Molecular modeling of this calcium complex using Gaussian03 software confirmed the assignments of the Raman vibrational bands.

Keywords: Bisphosphonate; Spectroscopy; Modeling; Cancer; Crystal structure

Introduction

Bone is a biogenic material made up of organic and inorganic components. The mineral content of bone comprises approximately 60–70 wt.% of the total dry bone weight while the remaining material is of organic nature (collagen, lipids, etc.). Bone mineral is an apatitic calcium phosphate containing 4–6% carbonate and small amounts of Na, Mg and other trace components [1]. Hydroxyapatite (HA, $[Ca_5(PO_4)_3(OH)]$) is thus widely used as a model of bone in many studies [2], [3], [4], [5], [6].

Macroanatomically, bone can be divided into two types, namely (i) compact (cortical) bone found in the middle portion of long and on the surface of flat bones; it is mostly responsible

for the structural integrity of bone, and (ii) trabecular (cancellous) bone, which is limited to the joints of bones and is mostly responsible for the transport of nutrients in bone. Bone, being a living tissue, is continually being regenerated. Trabecular bone accounts for 80% of the turnover, although it represents only 20% of the skeleton. On the other hand, cortical bone represents 80% of the skeleton but only accounts for a 20% turnover [7].

Bisphosphonates (BPs) are widely used in the treatment of degenerative bone diseases as pain palliative agents [8], and as transport agents for radio nuclides in the treatment of these bone diseases [9], [10], [11]. HEDP is the oldest known member of this class of compounds [12] and is used as the reference standard for potency studies of BPs with its own potency value set to one [13], [14]. Due to the different nomenclatures used in different scientific fields (organic and inorganic chemistry, biochemistry, etc.) for phosphorus compounds, this type of organophosphorus compounds (containing the P–C–P linkage) is also called a diphosphonate by biochemists although this term is more appropriate for phosphonic anhydrides (compounds containing P–O–P linkages) [15]. This results in many different names and abbreviations in the literature for the same bisphosphonate. The BP we refer to as HEDP is commercially known as etidronate or etidronic acid, but is also referred to as: HEB(or D)P(A) — 1-**h**ydroxy-**e**thyl(id)ene (or **e**thane)-1,1-**b**is(or **d**i)**p**hosphonic **a**cid; EHDPA — **e**thane-1-**h**ydroxy-1,1-**d**iphos**p**honic **a**cid, or H_4L where L^{4-} = EHDP™ — **e**thane-1-**h**ydroxy-1,1-**d**i**p**hosphonate.

HEDP has the ability to bind in a tridentate fashion to bone due to the presence of the hydroxyl group on the P–C–P carbon of the molecule. This tridentate interaction was postulated [16] and the well established as the OH group presence leads to enhanced chemisorption to the mineral [6]. The current paper investigated the reaction products of the interaction of HEDP with HA as a model of bone and therefore the bidentate coordinating nature of HEDP with calcium in the obtained $CaH_2L{\cdot}2H_2O$ crystal structure and in solution should not be confused with the possible tridentate interaction with bone or HA surface.

Although $CaHPO_4$ occurs in neither normal nor pathological calcifications (unlike its dihydrate, $CaHPO_4{\cdot}2H_2O$) [5] it showed similar chemical reactivity towards HEDP. A previous study [2] also postulates an 'adhesion–decalcification concept' which proposes the initial formation of HPO_4^{2-} during the action of carboxylic acids on HA and the subsequent decalcification thereof allowing Ca^{2+} (aq) to be available for complex formation. A similar process might be involved in the reaction of bisphosphonic acids with HA, and it was therefore decided to include it in this study as a source of aqueous HPO_4^{2-} for comparison with the reactions of HEDP with bovine bone and HA. As the study was done at the solution/solid reaction interface, using either $CaHPO_4$ or $CaHPO_4{\cdot}2H_2O$ as a source of HPO_4^{2-} (aq) would be chemically indistinguishable by Raman spectroscopy.

Raman spectroscopy has successfully been used for characterization of bone [3], HA (as a model of bone) [4], [17] and bisphosphonates (as active agents in bone disease treatment) [18], [19], [20], [21], [22], [23], [24]. Thus far, only one attempted Raman spectroscopic study on the interaction between a BP and bone or HA was found in the literature [25]. This is mainly due to occurrence of fluorescence, even when using Fourier Transform (FT) Raman with 1064 nm laser excitation which usually precludes electronic absorption, hence leading to the drastic reduction of fluorescence. A comparative study of conventional and FT-Raman spectroscopy of some calcium minerals showed strong fluorescence bands in the FT-Raman spectra of fluoroapatite, heated HA, tricalcium phosphate $Ca_3(PO_4)_2$, calcium hydrogenphosphate dihydrate $CaHPO_4{\cdot}2H_2O$, calcium hydroxide $Ca(OH)_2$ and calcium

carbonate $CaCO_3$ [26]. These fluorescence bands originate from impurities such as rare earth minerals contained in a particular structure or phase of the compound. With this in mind and due to the fact the HEDP is a colorless solid, it was decided to attempt the in situ Raman study by using a laser frequency in the visible part of the electromagnetic spectrum such as the 514.5 nm (green) line of an Argon ion laser and thus hopefully observe the interaction products/complexes formed between HEDP and bone or HA, without the problem of fluorescence.

Since HEDP is a tetraprotic acid (H_4L, L = $[CH_3C(OH)(PO_3)_2]^{4-}$), a variety of species can exist in solutions of different pH (e.g. H_4L, H_3L^-, H_2L^{2-}, HL^{3-} and/or L^{4-}) leading to the formation of many possible metal complexes. Formation of certain Ca–BP complexes, resulting from the reactions of bone or HA with BPs, was postulated but never proven [27], [28], [29], [30]. Isolation of such complexes formed would allow for their positive identification by other spectroscopic and diffraction techniques, such as NMR and XRD. NMR analysis can confirm whether the complex indicated in the solid state remains coordinated in both polar protic and aprotic solvents. Due to the complexity of the Raman vibrational spectra (arising from numerous bands and factors, such as overlapping of characteristic regions related to the different functional groups present) molecular modeling should be of great help in the assignment of these bands. These assignments are necessary to identify spectral shifts resulting from changes due to complexation (i.e. formation of new compounds). The only published solid state structure of $CaH_2L{\cdot}2H_2O$ was unsatisfactory as a result of certain atomic positional uncertainties and reported disorder [27]. It was thus decided to determine a more accurate single crystal structure to ensure optimal modeling results. A better understanding of structural aspects of BPs and their interaction with bone is of importance for future design of BP ligands included in radiopharmaceuticals used in treatment of bone cancer and other bone diseases.

Materials and methods

Materials

Hydroxyapatite (BIO-RAD, BIO-GEL®-HTP Gel) was obtained from Chemlab, Bryanston, South Africa, and its purity confirmed by powder XRD. HEDP was obtained from Fluka (purity > 97%) and used as received. $Ca(OH)_2$ (purity ≥ 95%) and H_3PO_4 (85% in H_2O) were obtained from Sigma-Aldrich. Samples of bovine bone were obtained from a local abattoir. The bone was treated with H_2O_2 and acetone according to [31]. All solutions were prepared using de-ionized water.

Synthesis

$CaHPO_4$: $Ca(OH)_2$ (3 g) was added to 4.86 mL 5 M phosphoric acid until neutralization at boiling point [15]. The precipitate was dried overnight at 120 °C and formation of the desired product was confirmed by powder XRD analysis.

$Ca(CH_3C(OH)(PO_3H)_2){\cdot}2H_2O$ i.e. $Ca(H_2L){\cdot}2H_2O$: Solid $Ca(OH)_2$ was added to an HEDP solution such that the molar ratio was 1:1. The desired complex precipitated out immediately as the $Ca(H_2L)$ complex is sparingly soluble at higher pH values (between 2 and 6) resulting from the addition of $Ca(OH)_2$; it was washed with de-ionized water and left to air dry. The compound was confirmed by powder XRD. The single crystal used for our structural

determination crystallized from a solution containing 25 mg HA (completely dissolved) in 3 mL of 0.5 M HEDP (pH 0.686) at pH 0.817.

Analysis

Raman spectroscopy

Raman spectra of the samples were excited with the 514.5 nm (green) line of a Coherent Innova 300 Argon ion laser. An Olympus confocal microscope with a 50× objective was used to focus the laser light on a solid sample or a solid–liquid interface. The scattered light was dispersed and recorded by means of a Dilor XY multichannel Raman spectrometer equipped with a liquid nitrogen-cooled Wright Generation 1 CCD detector. The spectral resolution was 3 cm^{-1}, while laser output powers at the source (300–500 mW) and integration times (30–120 s) were varied to obtain the best possible spectra (concerning signal to noise ratio). Three spectral accumulations were averaged and the software used for data processing was Labspec Version 3.03.

Solid samples of each of the materials (bone, HA, $CaHPO_4$ and HEDP) were analyzed on the microscope slides by micro Raman spectroscopy. Bone, HA and $CaHPO_4$ required a higher laser power to obtain spectra comparable to those of HEDP. Some of the Raman bands have shown variable intensities at different spots of the same sample, probably due to variable crystal orientation. With further grinding of the sample one would expect that the intensity variations might be diminished, but this did not occur. Macro Raman spectroscopy (obtained using a 50 mm lens) was attempted as this would give an averaged spectra of the bulk material, free of intensity variations, but the band intensities were much weaker therefore fewer bands were observed.

In situ Raman measurements of the interactions of HEDP with bone, HA and $CaHPO_4$

In order to simulate bone treated by the HEDP drug, HEDP solutions (0.5–0.005 M) were added dropwise onto the solid bone, HA or $CaHPO_4$ placed on the microscope slide, until the whole solid surface was covered with solution. A crystalline material started to form on the HA (or $CaHPO_4$) as the HEDP solutions were added and this could be observed under the microscope (50× magnification). A series of spectra were recorded until no further change was observed.

Single crystal XRD

The single X-ray crystal structure analysis was performed using data collected at 20 °C on a Siemens P4 diffractometer fitted with a Bruker 1K CCD detector and SMART control software [32] using graphite-monochromated, Mo-Kα radiation by means of a combination of phi and omega scans. Data reduction was performed using SAINT+ [32] and the intensities were corrected for absorption using SADABS [32]. The structure was solved by direct methods using SHELXTS [32] and refined by full-matrix least squares using SHELXTL [32] and SHELXL-97 [33]. The crystal data and refinement details for $Ca(CH_3C(OH)(PO_3H)_2)\cdot 2H_2O$ are summarized in Table 1. All the hydrogen atoms were located experimentally and were included in the refinement without any constraints except for the half-occupancy H(5) and H(6) atoms which represent a disordered hydroxyl group bonded to P(2) and equally distributed between O(5) and O(6). H(5) and H(6) were allowed to ride on O(5) and O(6) respectively with $d_{O–H}$ = 0.82(1) Å and the P–O–H angle tetrahedral

and allowed to rotate about the corresponding O–P bond. The isotropic displacement parameters of H(5) and H(6) were fixed at 1.5 times the equivalent isotropic displacement parameter of O(5) and O(6) respectively. Drawings of the structure were produced using Ortep-3 for Windows (version 1.076) [34], Mercury (version 1.4.2) [35] and POV-Ray for Windows (version 3.6) [36].

Table 1
Crystal data collection and refinement details for $CaH_2L{\cdot}2H_2O$

Identification code	lp01_abs	
Empirical formula	$C_2\ H_{10}\ Ca\ O_9\ P_2$	
Formula weight	280.12 g/mol	
Temperature	293(2) K	
Wavelength	0.71073 Å	
Crystal system	Triclinic	
Space group	PT	
Unit cell dimensions	a=6.9499(6) Å	α=92.7330(10)°
	b=7.5961(6) Å	β=106.3140(10)°
	c=9.7000(8) Å	γ=112.4250(10)°
Volume	447.33(6) Å^3	
Z	2	
Density (calculated)	2.080 Mg/m^3	
Absorption coefficient	1.087 mm^{-1}	
F(000)	288	
Crystal size	0.30 mm×0.22 mm×0.18 mm	
Theta range for data collection	2.95 to 26.41°.	
Index ranges	$-5\le h\le 8$, $-9\le k\le 4$, $-11\le l\le 10$	
Reflections collected	2442	
Independent reflections	1622 [R(int)=0.0200]	
Completeness to theta=25.00°	97.7%	
Absorption correction	Semi-empirical from equivalents	
Maximum and minimum transmission	0.822 and 0.707	
Refinement method	Full-matrix least-squares on F^2	
Data/restraints/parameters	1622/0/165	
Goodness-of-fit on F^2	1.083	
Final R indices [I>2sigma(I)]	R1=0.0331, wR2=0.0915	
R indices (all data)	R1=0.0336, wR2=0.0920	
Extinction coefficient	0	
Largest different peak and hole	0.844 and −0.472 e.Å^{-3}	

Powder-XRD

Powder-XRD analysis was performed on a PANalytical X'Pert automated diffractometer using Co–Kα radiation. An X'Celerator detector was used and data collected for 2θ angle from 5.0° to 90.0°.

NMR spectroscopy

Solution NMR spectra were recorded on a Bruker ARX-300 spectrometer. ^{1}H and ^{31}P NMR spectra were recorded at 300.135 and 121.46 MHz, respectively. The signal of the deuterated DMSO-d_6 at 2.49 ppm was used as a reference in the ^{1}H spectrum, whereas ^{1}H measurements in D_2O were referenced using an internal standard probe of $CDCl_3$ with an RS value of 4100.56 Hz. ^{31}P NMR spectra were referenced to 85% H_3PO_4 in H_2O at 0.00 ppm.

UV–Visible spectroscopy

The solid state UV–Visible spectrum of $CaH_2L{\cdot}2H_2O$ was obtained by dispersing the sample in a KBr pellet for a weight ratio of 1:3. A pure KBr pellet was used as the reference. The spectrum was recorded on a Perkin Elmer Lambda 25 UV–VIS Spectrometer using a Labsphere RSA-PE-20 Reflectance Accessory to record the spectral reflectance of the solid sample in the region 190–1100 nm.

Molecular modeling

The starting conformation coordinates of the $CaH_2L{\cdot}2H_2O$ were used from the crystallographic structure solution without further structural optimization and comprised the content of one unit cell. The computation of the vibrational spectra (Raman, IR) by Gaussian03 [37] software was accomplished by employing standard Hatree–Fock (HF) methods. This method was selected based on initial evaluation of a various Hatree–Fock and Density Functional Theory (DFT) basis sets at different levels of theory showing satisfactory comparisons for similar systems as modeled for the region below 2000 cm^{-1}. The basis set used was therefore HF/6-311G++(d,p). The scaling factor used was 0.9051 [38].

Results and discussion

Raman spectroscopic study

Solid state UV–VIS spectroscopy of the HEDP indicated extensive absorption above 730 nm justifying our choice of using the 514.5 nm over the 1064 nm (FT-Raman) laser line as was previously reported in the literature [25].

The two macroanatomical bone types, trabecular (cancellous) and compact, (cortical) showed different Raman spectra. The spectral differences are ascribed to increased presence of calcium phosphate apatitic mineral in the compact bone, while the organic components (collagen, remaining lipids and blood) are dominant in the porous bone. Fig. 1 shows the comparison of the Raman spectra obtained in this study of the two types of bone with HA and $CaHPO_4$. The similarities of HA with compact bone can clearly be seen (bands between 400 and 1100 cm^{-1}), indicating the structural similarities of the two as was previously reported [3], [39]. Also, the organic component found mostly in parts of the trabecular bone is apparent from the bands above 1100 cm^{-1} which arise from lipids, collagen and other organic

bone components that swamp the strongest peak of the HA at 960 cm^{-1}. The full assignments for HA and $CaHPO_4$ from the literature are summarized in Table 2, and a comprehensive assignment regarding Raman spectra obtained on bone can be found in [3].

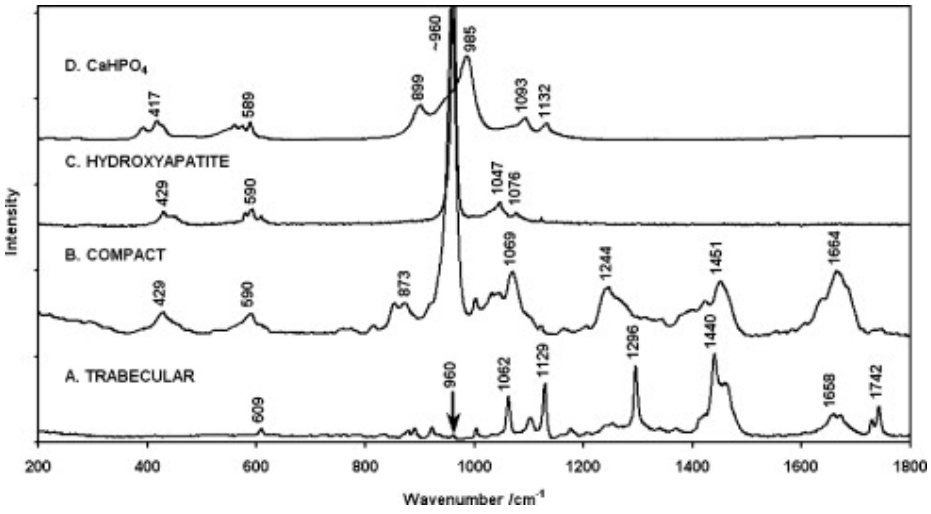

Fig. 1. The Raman spectra of (A) trabecular bone, (B) compact bone, (C) hydroxyapatite and (D) $CaHPO_4$ for the region 200–1800 cm^{-1} showing the similarity of bone with hydroxyapatite and the highly organic nature of trabecular bone. Only bands of strong intensity are labeled to serve as a guide, but all bands have been assigned (see Table 2) for hydroxyapatite and $CaHPO_4$.

Upon addition of the HEDP solutions (at various concentrations) to the bone, HA(s) or $CaHPO_4$(s), two distinguishable calcium complexes could be observed using Raman spectroscopy. For both these calcium complexes and HEDP many vibrational bands are present as can be seen in Fig. 2. It was found that each compound has three non-overlapping bands which can be used to monitor the formation of the calcium complexes relative to HEDP. These bands are at 627, 972 and 1036 cm^{-1} for HEDP; at 658, 946 and 1088 cm^{-1} for the unknown calcium complex; and at 641, 963 and 1072 cm^{-1} for $CaH_2L{\cdot}2H_2O$. The first band (627, 658, 641 cm^{-1}) for each compound is confidently assigned to the νC–P bond stretch [24], [40]. The second band (972, 946, 963 cm^{-1}) is assigned to the symmetric ν^{s}P–O(H) stretching vibration judging by its shift with pH [20], [21], whereas the third band (1036, 1088, 1072 cm^{-1}) is assigned to both δPO–H bending and ν^{as}P–OH asymmetric stretching vibrations [20], judging by its unusual increase in intensity compared to the second group of bands [20], [21], [40]. The dramatic shifts within the second and third group of bands can be explained by the changes in the P–O bond order [41] due to the different modes of coordination of the Ca^{2+} ion with the phosphorus bonded oxygen atoms. Many other bands of lower intensity are also indicative of the compounds present, but some are overlapping or may not be observed at lower concentrations and could therefore be used only as a secondary means of confirmation (if they are observed). The PO vibrational region [40] (~ 910–1300 cm^{-1}) is rich in bands for all three compounds and also overlaps with the tertiary carbon COH vibrational region [40] (~ 1100–1210 cm^{-1}), further complicating assignments of some of the bands of lower intensity. Only the abovementioned bands will further be used in the discussion.

Table 2
Raman band positions and vibrational assignments for bone, HA, $CaHPO_4$, HEDP, $CaH_2L{\cdot}2H_2O$ and the unknown Ca complex for the region 200–4000 cm^{-1}

Vibrational assignments	Solid 'substrates'			Solid compounds			
	Bone [a]	$CaHPO_4$ [b]	HA [c]	HEDP [d]	Ca-complex	$CaH_2L{\cdot}2H_2O$ experimental	$CaH_2L{\cdot}2H_2O$ calculated [e]
Probable lattice vibrations		140 w			114 vw	110 vw	
		180 w				121 vw	
		224 w			144 vw	149 w	
		268 w				170 sh	
					185 vw	182 w	
νOH....O				205 w		204 w	263, 273 vw
				241 s	223 vw	228 w	
δ C–C				274 s	277 m	254 vw	
				289 m		301 m, sh	
				327 sh	326 w	313 m	311 w
δ OPO				344 vs	345 w	342 s	332 w
					383 w	360 m	355 w
				408 m,br		412 w	394 m
δ^{as} PO_4^{3-}	429	392 m	431 m				
		417 m	447 m				
		428 m, sh					
				445 w,sh		457 m	459 m
δ OPO				466 m	487 w	482 w, sh	494 vw
				497 m		506 w	513 w
				525 w, br	529 w-m	528 m	559 vw
δ^{as} PO_4^{3-}		539 m					
		560 m	580 m				
	590	573 m	592 m				
		589 m	608 w				
					557 w	543 m	589 vw
νC–P				627 vs,br	658 s	641 vs	643 vs
						742 w, br	756 m
νC–C–O				824 m	819 w	828 w	871 vw
ν^{as} PO_4^{3-}		899 s					
νC–O–H				917 m	897 m	898 m	909 vs
ν^{s} P–O(H)				936 m	920 m,sh	916 w	929 s
				972 vs	946 s	963 m,br	1000, 1028 s
ν^{s} PO_4^{3-}	958	958 s,sh	962 vs				

		985 vs					
ν^{as} PO_4^{3-}	1044	1065	1047 m				
		1093					
		1132					
νP–O(H)				1036 s,br	1049 m	1057 sh	1054 m
δ PO–H/ν^{as} P–O(H)				1074 m, br	1088 s	1072 vs	1076 w
ν^{as} PO_4^{3-}			1076 w				
δ CO–H					1134 m	1122 m	1116 w
νP=O/δ^{π} POH				1141 m,br	1160 m	1158 m	1141 s
					1188 sh	1172 sh	1185 vw
				1228 w		1207 w	
						1347 w	
δ^{s} $C(CH_3)$				1375 w	1374 w	1373 vw	
						1385 w	
δ^{as} CH_3				1451 m	1456 m	1452 s	
				1462 m		1462 s	
νPO–H				2737 w	2725 w	2743 w	
ν^{s} CH_3				2882 m	2882 sh	2883 m	
					2887 m		
				2911 m	2921 sh	2919 w	
ν^{as} CH_3				2951 vs	2953 vs	2950 vs	
				2998 s		2983 sh	
					2999 s,sh	2991 s	
					3006 sh	3001 w	
				3012 m	3010 vs	3020 m	
				3031 w			
ν O–H/H_2O					3222 m	3224 vw,br	
						3354 m-w	
						3409 sh	
ν O–H/HA			3578 s		3571 m		

ν: stretching mode, δ: deformation mode.

s: symmetrical, as: anti-symmetrical.

vw: very weak, w: weak, m: medium, s: strong, vs: very strong, sh: shoulder.

[a]Only the bands observed of HA are listed for bone. The full assignments for the organic component can be found in [3].
[b]Ref. [47].
[c]Ref. [17].
[d]Refs. [20], [21], [24].
[e]Assignments regarding lattice vibrations could not be done from the generated data and assignments are further complicated by solid state vibrational splitting, and thus could not confidently be done for certain observed vibrational bands.

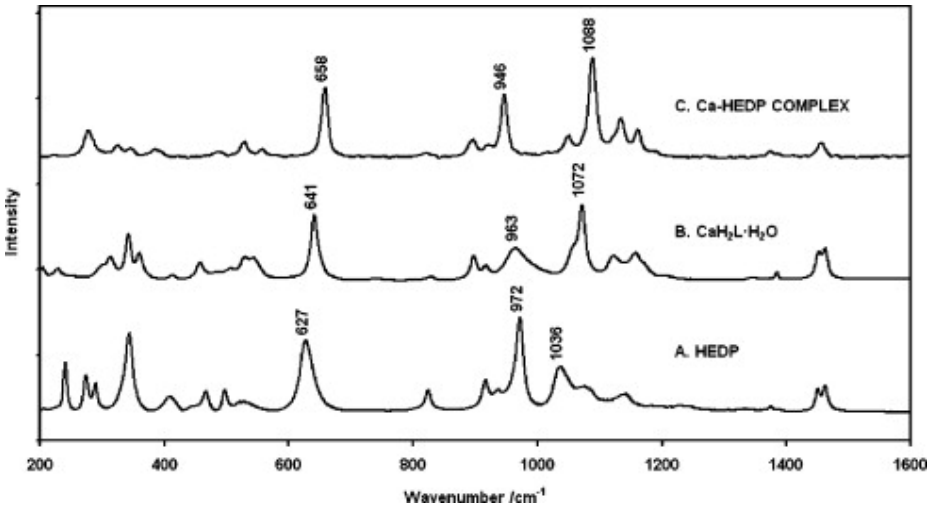

Fig. 2. Comparative spectra of (A) HEDP, (B) the $CaH_2L \cdot 2H_2O$ complex and (C) the unknown Ca complex for the region 200–1600 cm^{-1}. Only the bands that have been identified as uniquely indicative of the compound present have been labeled, but the full Raman spectra of all three have been assigned (see Table 2).

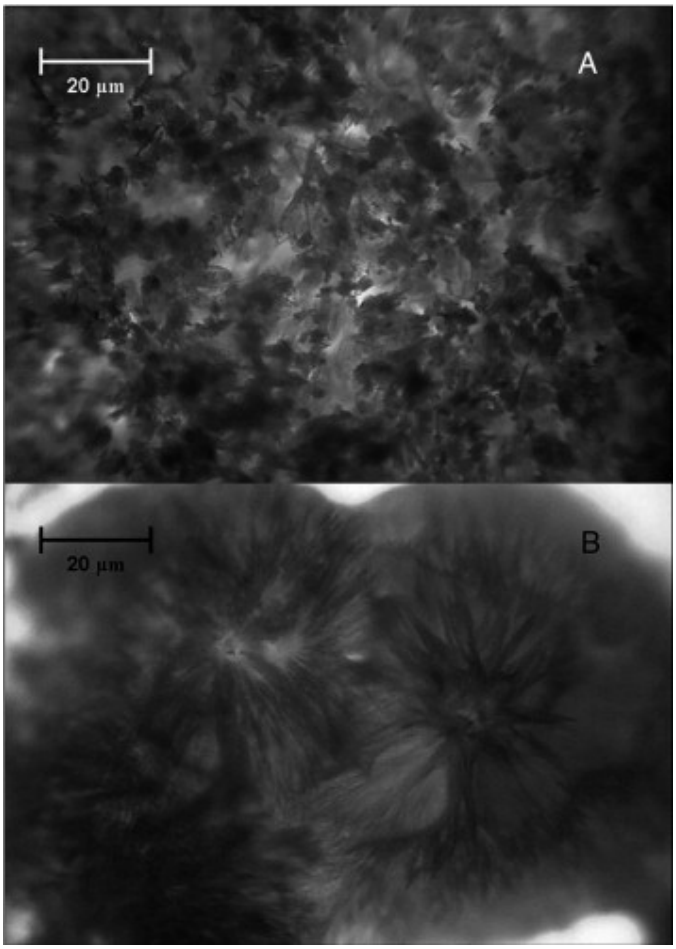

Fig. 3. Optical light microscopy of hydroxyapatite crystals (A) before the addition, and (B) after the addition of 0.5 M HEDP (both 45× magnification).

It appears that HEDP (between 0.5 and 0.005 M) reacts with bone, HA(s) and $CaHPO_4$(s) in the same way, forming needle-like crystals orientated in fused spherical shapes (Fig. 3). The Raman spectra of the products formed during the above reactions are very similar as can be seen in Fig. 4. This indicates that HEDP reacts with the Ca^{2+} ion present in all three of the solid materials (bone, HA and $CaHPO_4$), thus forming similar Ca complexes (Fig. 3). One might conclude that HA can be used as a substitute in studying interactions with chemical compounds investigated here.

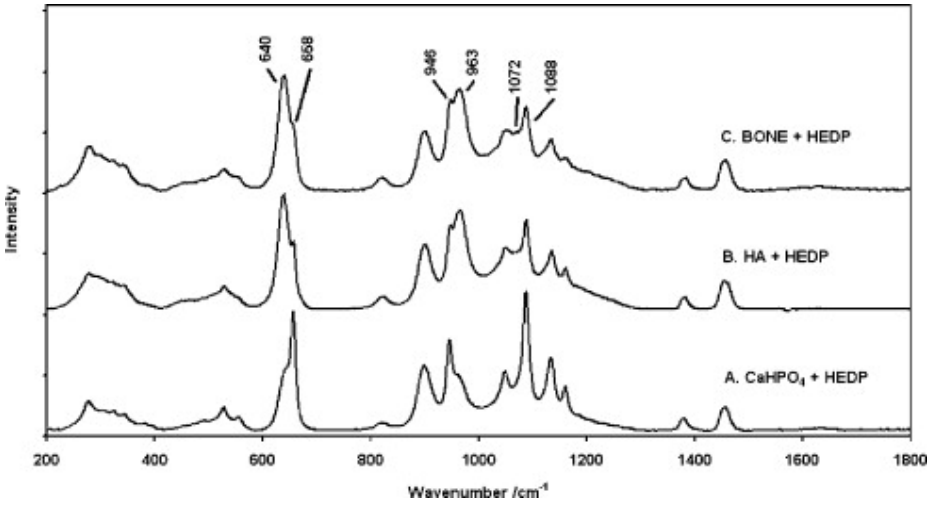

Fig. 4. The comparison of the Raman spectra for the region 200–1800 cm^{-1} of the reactions of the HEDP with (A) $CaHPO_4$, (B) HA and (C) bone showing the formation of similar reaction products. The important bands used to discern between the two Ca complexes are indicated. 640, 963 and 1072 cm^{-1} are assigned to the $CaH_2L{\cdot}2H_2O$ complex and 658, 946 and 1088 cm^{-1} are assigned to the unknown Ca complex.

We have established that when HEDP is present at low concentrations (multiple drops of 0.005 M solution of pH ~ 2.2, or one drop of 0.5 M solution of pH ~ 0.7 added to the HA(s)) then the unknown calcium complex, $Ca_xH_yL_z{\cdot}nH_2O$ (bands at 658, 946 and 1088 cm^{-1}), is formed first at the solid–liquid interface. Upon the addition of a sufficient amount of HEDP, $CaH_2L{\cdot}2H_2O$ starts to form and its formation can be monitored by the appearance of the bands at 641, 963 and 1072 cm^{-1} in the Raman spectrum showing that both calcium complexes are now present. Similar observations were made when $CaHPO_4$(s), instead of HA(s), was treated with HEDP solutions. However, if the same small volume of 0.5 M HEDP is placed on the bone surface then two calcium complexes are formed simultaneously: the unknown $Ca_xH_yL_z{\cdot}nH_2O$ and $CaH_2L{\cdot}2H_2O$. The above findings suggest that formation of these two complexes is a function of the pH of a solution at the solid–liquid interface (the reaction zone) with the CaH_2L complex being formed only under more acidic conditions. In general, this is in agreement with the successive and pH-dependent formation of several calcium complexes with HEDP in a solution [42] where three complexes were identified by Glass Electro Potentiometric (GEP) studies, namely $CaHL^-$, Ca_2L and CaL^{2-} for which the overall stability constants (log β) were reported to be 13.17, 9.53 and 5.34, respectively. The fact that CaH_2L was not found by GEP and the unknown complex was formed at lower HEDP concentrations prompted us to use computer modeling of a hypothetical solution composition using the reported data [42] and an assumed (guessed) stability constant of the complex CaH_2L. We allowed the total Ca^{2+} (aq) concentration to vary in a wide range, between 1×10^{-3} and 1×10^{-7} M. This is due to the fact that the stock HEDP solution was calcium-free and most of calcium leached from the solid phase (HA, bone or $CaHPO_4$) was

instantly involved in the complex formation reaction with HEDP, and formation of these solid complexes was observed by us — see Fig. 3. From the results generated by computer modeling (not shown here) it appeared that the overall stability constant (log β) for the CaH_2L should be approximately 18; only a small selection of the species distribution diagrams is presented here to facilitate the discussion that follows — see Fig. 5. The analysis of the species distribution diagram shown in Fig. 5A (composition of a solution was computed for experimental conditions and stability constants of $CaHL^-$, Ca_2L and CaL^{2-} as reported in [42] with an inclusion of CaH_2L, log $\beta = 18.5$) explains why the complex CaH_2L could not be established by GEP. This complex (marked as 1 in Fig. 5A) is formed first (at the lowest pH values) but (i) only to a small extent (only a small portion of the total calcium dissolved is in a solution) and (ii) in the pH range where the H_2L^{2-} form of the HEDP ligand is by far the dominant ligand species present. It means that according to the following reaction,

$$Ca^{2+}+H_2L^{2-}\rightarrow CaH_2L$$

there is no proton involved, and hence there is no change in the total free proton concentration in a solution when this complex is formed. GEP is the most powerful and versatile analytical technique used in the study of metal complexes but it can only work when the free proton concentration varies due to the complex formation reaction. Complexes $CaHL^-$ and Ca_2L (marked as 2 and 3, respectively, in Fig. 5A) start to form almost simultaneously in the pH range between 5 and 6, but Ca_2L develops to a much larger extent. When the total calcium concentration is decreased down to 1×10^{-6} M and the total ligand concentration increased to 0.005 M (most likely the experimental conditions we had for the lower HEDP concentration) then the solution composition changes dramatically — see Fig. 5B. It is clear that at the lower total metal ion concentration the polynuclear complex Ca_2L is not formed to any significant concentration level (not shown in Fig. 5B at all). Now $CaHL^-$ is the major calcium complex with only a small fraction of CaH_2L formed. The results of modeling generated for 0.5 M HEDP (see Fig. 5C) document our experimental results when the formation of CaH_2L at very low pH was observed and a single crystal of this complex was made. Even at a high total metal ion concentration (1×10^{-3} M) there is no evidence of the Ca_2L formation. The above is in total agreement with our experimental observations discussed above and strongly suggests that $CaHL^-$ is the unknown complex mentioned above. We were not able to grow a single crystal containing $CaHL^-$ to confirm our supposition fully.

In an effort to increase the yield of the postulated $CaHL^-$ complex the pH of a solution containing HEDP was adjusted upwards by addition of $Ca(OH)_2$(s). If the molar ratio of $Ca(OH)_2$:HEDP was 1:1, the complex $CaH_2L{\cdot}2H_2O$ was precipitated (as confirmed by XRD), while a ratio of 2:1 resulted in a mixture of complexes that could not be resolved by XRD. It would be invaluable if all the calcium complexes with HEDP could be synthesized and characterized using X-ray diffraction techniques.

The only Ca complex synthesized as well as characterized by XRD to date is $CaH_2L{\cdot}2H_2O$. It was crystallized from an initial solution of 25 mg HA in 3 mL of 0.5 M HEDP resulting in a solution of pH 0.817. The crystals formed after standing for about a month, and their Raman spectrum can be seen in Fig. 2B. The bands of the other Ca complex were observed in the reaction of low concentrations of HEDP with the three solids, but this complex could not be isolated successfully (Fig. 2C).

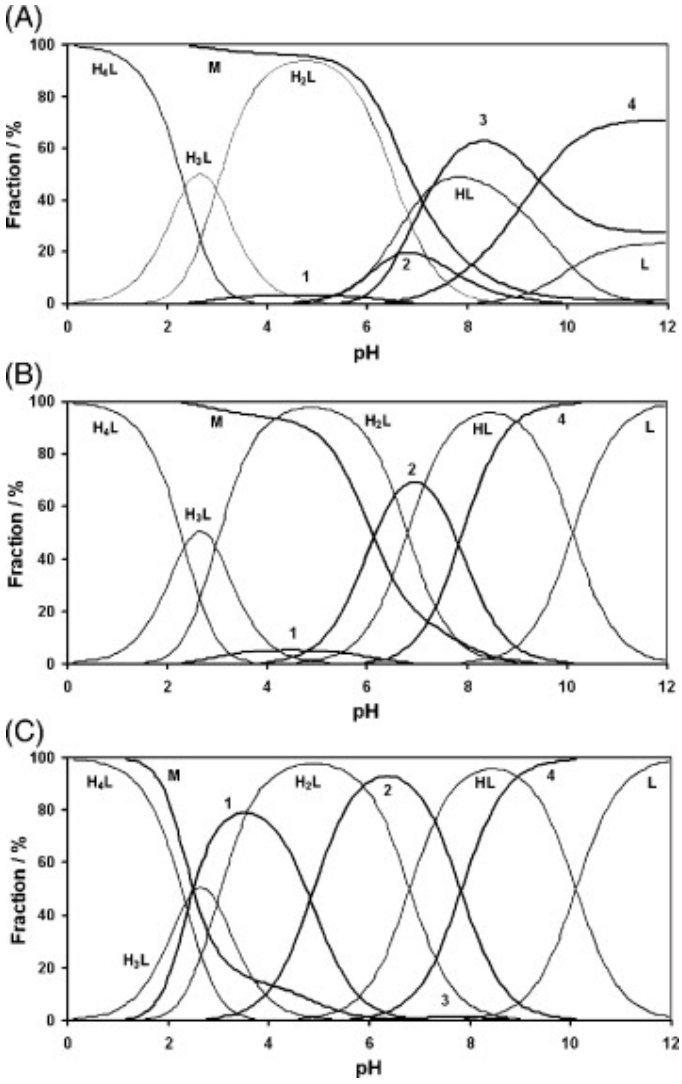

Fig. 5. Species distribution diagrams computed for a hypothetical Ca–HEDP metal–ligand system with an assumption made that all species are totally soluble under assumed experimental conditions. Protonation constants [42]: log K_1 = 10.11, log K_2 = 6.81, log K_3 = 2.97, log K_4 = 2.35. Overall stability constants for ML (4), M_2L (3) and MHL (2), as log β, from [42]: 5.34, 9.53 and 13.17, respectively. (A) $[L_T] = 1 \times 10^{-3}$ M, $[M_T] = 9 \times 10^{-4}$ M, overall stability constant, as log β, for MH_2L (1) set to 18.5. (B) $[L_T] = 5 \times 10^{-3}$ M, $[M_T] = 1 \times 10^{-6}$ M, overall stability constant, as log β, for MH_2L (1) set to 18.0. (C) $[L_T] = 5 \times 10^{-1}$ M, $[M_T] = 1 \times 10^{-3}$ M, overall stability constant, as log β, for MH_2L (1) set to 18.0.

Hatree–Fock (HF) methods were chosen for the molecular modeling of $CaH_2L \cdot 2H_2O$, even though these methods do not take dynamic electron correlations into account [43]. This was done as no initial geometrical optimization was performed on the structure as determined from single crystal X-ray diffraction, resulting in a less time consuming approximation. Furthermore, when initial test calculations were done on a simpler, single molecule to compare HF and DFT methods in combination with various basis sets, it was found that the scaling factor required for the computed vibrational frequencies was the only dramatic difference between the two methods. After applying a suitable scaling factor to the raw data obtained from each of the two methods the results were comparable. Thus, the HF/6-311G++(d,p) set was selected, with the use of a scaling factor of 0.9051 [38]. Because HF

methods do not show a non-linear relation between the calculated and theoretical vibrational frequencies, such as the DFT methods [44], only wavenumbers below 2000 cm^{-1} were considered for assignments. Assignments of experimental Raman bands observed above 2000 cm^{-1} could be done from literature sources. All these assignments are presented in Table 2.

Crystallographic studies

When Uchtman [27] first reported the crystal structure of $CaH_2L \cdot 2H_2O$, the hydrogen positions were not well determined experimentally. This is not at all unusual for bisphosphonate crystal structures [45]. In order to generate a theoretical vibrational spectrum using HF methods a starting conformation of acceptable accuracy was required. The single crystal data obtained in this work are summarized in Table 1. Fig. 6 is an Ortep/POV-Ray drawing of the asymmetric unit which, in addition, shows the full coordination geometry of the Ca atom and the hydrogen bonding in the structure. The fully protonated HEDP (H_4L) molecule has a σ-plane defined by the C(2)–C(1)–O(7) atoms and can obtain C_s as its highest point group symmetry. As in all the other published structures containing either H_3L, H_2L, HL and/or L [45], the H_2L moiety adopts a C_1 conformation in the crystal structure due to hydrogen bonding [45]. The Ca atom has eight coordinates, with Ca–O bond lengths in the range 2.3578(17)–2.5921(18) Å, mean 2.47 Å. This is comparable to the Ca–O bond length of 2.41 Å in calcium oxide at 298 K [46]. The structure forms a network of infinite 2-dimensional layers parallel to the 0,0,1 face of the unit cell with the units within each layer linked via bridging coordination of the Ca atoms by the O(8) water molecules and the H_2L moieties, and also via extensive intermolecular hydrogen bonding. Pairs of Ca atoms are bridged by two symmetry related H_2L moieties: each Ca is bonded by a 6-membered chelate ring, via O(1) and O(4), to one H_2L and by a 5-membered chelate ring, via O(2) and O(7) to the second H_2L resulting in a Ca….Ca separation of 5.4237(10) Å. Also, O(2), together with a symmetry related O(2) in a further H_2L moiety, forms coordination bridges to another Ca atom. Additionally, two symmetry related O(8) water molecules form coordination bridges to a further Ca atom. The 4-membered coordination rings are also formed, $(Ca(1)–O(2))_2$ and $(Ca(1)–O(8))_2$, and they result in Ca⋯⋯Ca separations of 3.7907(9) Å and 4.1334(9) Å respectively. Thus each Ca atom is linked by coordination bridges to three other Ca atoms to form infinite 2-dimensional network layers. These layers are linked via hydrogen bonds between O(5)–H(5) and O(5∗∗), O(6)–H(6) and O(6∗) and between O(9)–H(9B) and O(6##) (see Fig. 6 for the symmetry operations referenced by ∗, ∗∗ and ##). As the proton in the P(2) phosphonyl group is equally disordered between O(5) and O(6), there is, presumably, one hydrogen bond formed for each O(*n*)–H(*n*)⋯⋯O(*n*) link (*n* = 5, 6) with one O atom protonated and acting as the donor and the other not protonated and acting as the acceptor. All the other hydrogen bonds (see Fig. 6) occur within the layers. A list of hydrogen bonding distances can be found in Table 3. To ensure that the experimentally obtained XRD powder pattern could be used as confirmation of the synthesis of the $CaH_2L \cdot 2H_2O$ complex, a theoretical pattern was generated from the experimentally determined single crystal structure. The experimentally measured and theoretically generated powder patterns do match and allowed for the powder pattern to be indexed.

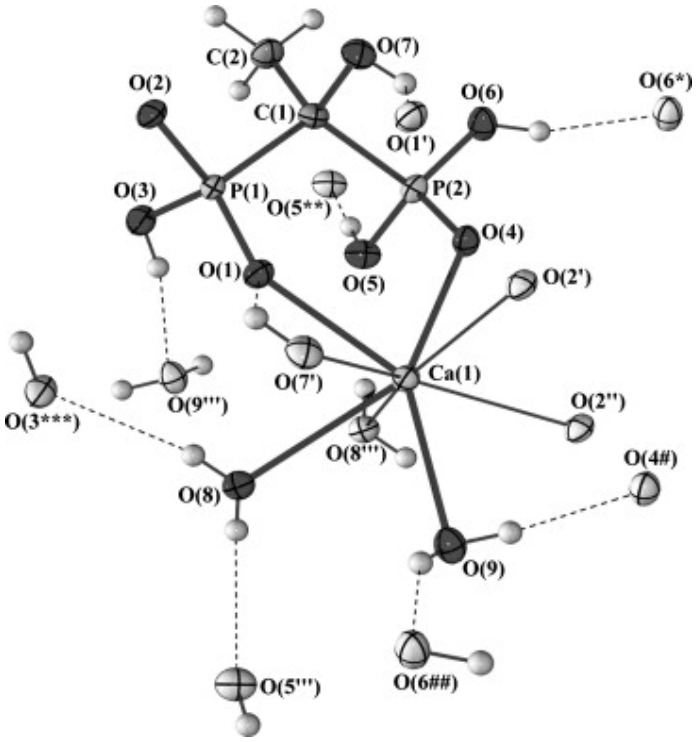

Fig. 6. An Ortep/POV-Ray drawing showing the asymmetric unit of the crystal structure of $Ca(CH_3C(OH)(PO_3H)_2)\cdot 2H_2O$ plus additional O atoms to complete the coordination around Ca(1) and acceptor O atoms involved in the network of hydrogen bonds. The additional O atoms are shown in a light color. Displacement ellipsoids are shown at the 50% probability level. The symmetry operations are: $'=\bar{x}, \bar{y}+1, \bar{z}$; $''=x+1, y, z$; $'''=\bar{x}+1, \bar{y}, +2, \bar{z}$; $*=\bar{x}+1, \bar{y}+1, \bar{z}+1$; $**=\bar{x}+1, \bar{y}+2, \bar{z}+1$; $***=\bar{x}, \bar{y}+2, \bar{z}$; $\#=\bar{x}+1, \bar{y}+1, \bar{z}$; $\#\#=x, y, z-1$.

Table 3
Selected hydrogen bonds (Å) for $CaH_2L\cdot 2H_2O$

O–H···A	d(O–H)	d(H···A)	d(O···A)	O–H–A (°)
O(3)–H(3)···O(9‴)	0.78(4)	1.94(4)	2.702(3)	168(4)
O(5)–H(5)···O(5**)	0.82	1.70	2.513(3)	173
O(6)–H(6)···O(6*)	0.82	1.75	2.537(3)	159
O(7)–H(7)···O(1′)	0.82(4)	2.16(3)	2.729(2)	127(3)
O(8)–H(8A)···O(5‴)	0.68(4)	2.10(4)	2.775(3)	167(4)
O(8)–H(8B)···O(3***)	0.72(4)	2.10(5)	2.804(3)	166(4)
O(9)–H(9A)···O(4#)	0.79(4)	1.91(4)	2.689(2)	167(4)
O(9)–H(9B)···O(6##)	0.75(4)	2.10(4)	2.787(3)	152(4)

The symmetry operations can be found in Fig. 6.

NMR studies

Comparative solvent NMR studies of the $CaH_2L\cdot 2H_2O$ complex and $HEDP\cdot H_2O$ were done in DMSO-d_6 and D_2O. To ensure that no interference was experienced with residual water in DMSO-d_6 a blank was run; no detectable water was observed. The Ca complex is only slightly soluble in both solvents, and therefore all the observed signals were weak. All the

observed values for the ^{1}H and ^{31}P spectra are listed in Table 4. Due to the high rate of exchange of acidic protons, neither PO**H** nor CO**H** signals are observed in the ^{1}H NMR spectrum for HEDP in D_2O. However, both the PO**H** and CO**H** signals were observed at 8.4 and 2.0 ppm, respectively, for the Ca complex in D_2O. This shows that the rates of exchange of these two protons are dramatically different, with proton exchange on the Ca complex being sufficiently slower, making the process observable on the NMR timescale. This indicates that the complex does exist in an aqueous solution. The O**H**$_2$ signals are observed at 3.8 and 3.7 ppm for HEDP and $CaH_2L{\cdot}2H_2O$, respectively, in DMSO-d_6. The fact that the expected PO**H** signal was not observed for $CaH_2L{\cdot}2H_2O$ could be as a result of the low solubility of the complex in the solvent(s). Also, no Ca–O**H**$_2$ signal was observed in D_2O, probably because of H_2O molecules rapidly exchanging with D_2O molecules when coordinating with the Ca of the $CaH_2L{\cdot}2H_2O$ complex.

Table 4
^{1}H and ^{31}P NMR Data for $HEDP{\cdot}H_2O$ and $CaH_2L{\cdot}2H_2O$

$HEDP{\cdot}H_2O$	δ (D_2O)[a]	J (Hz)[b]	δ (DMSO-d_6)[a]	J (Hz)[b]
POH	–	–	7.9 (b)	–
COH	–	–	2.1 (s)	–
CH_3	1.6 (t)	$^{3}J_{H,P}$=16.0	1.4 (t)	$^{3}J_{H,P}$=15.8
OH_2	–		3.8 (b)	–
P	22.9 (t)	$J_{P,C}$=150.0	25.2 (t)	$J_{P,C}$=148.8
$CaH_2L{\cdot}2H_2O$				
POH	8.4 ? (s)	–	–	–
COH	2.0 ? (s)	–	1.2 ? (s)	–
CH_3	1.5 (t)	$^{3}J_{H,P}$=15.2	1.4 (t)	$^{3}J_{H,P}$=15.8
OH_2	–	–	3.7 ? (b)	–
P	21.7 (s)	–	25.2 (s)	–

b: broad, s: singlet, t: triplet.
[a] δ: Signal shift measured in ppm relative to references as set out under NMR spectroscopy.
[b] J: coupling constants measured in hertz (Hz).

To summarize all these results, it has been experimentally demonstrated that micro Raman spectroscopy with the 514.5 nm laser line (used for the first time in this kind of study) can successfully be used to investigate the interactions of HEDP (as a model of BP) with bone, HA (as a model of bone) and $CaHPO_4$, because interference caused by fluorescence was significantly diminished. All three of these compounds gave the same reaction products with HEDP (H_4L). The $CaH_2L{\cdot}2H_2O$ complex (formed at extremely low pH values) was identified as one of the two complexes observed on the surface of the bone upon treatment with HEDP solution. Modeling of solution composition (using the data from reference [42]): (i) strongly supports our supposition that $CaHL^{-}$ is the other complex formed at higher pH values and (ii) explains why the stability constant for CaH_2L could not be reported in the literature [42].

Accurate structural determination for $CaH_2L{\cdot}2H_2O$ assisted in the generation of a more confident theoretical vibrational spectrum, resulting in the assignments of the bands of the complicated Raman spectrum. The theoretical vibrational spectrum of $CaH_2L{\cdot}2H_2O$ was computed using Gaussian03 software by employing the HF/6-311G+(d,p) basis set, and it was not necessary to employ DFT methods when results below 2000 cm^{-1} were of interest. It

was also shown by means of NMR spectroscopy that the complex CaH_2L does not dissociate to a large degree in solution.

The combination of Raman spectroscopy (solid, or solid–liquid interface) with solution chemistry together with NMR, structural and modeling studies proved to be a powerful multidisciplinary tool in the study and understanding of the interactions of HA (as a substitute for bone) and BPs, specifically HEDP in this case. This shows an innovative approach in using various instrumental techniques in the study of BPs (and possibly radiopharmaceuticals) to further understand factors controlling the potency of BPs and their complexes.

References

[1] Constantz BR, Ison IC, Fulmer MT, Poser RD, Smith ST, Van Wagoner M,Ross J, Goldstein SA, Jupiter JB, Rosenthal DI. Skeletal repair by in situ formation of the mineral phase of bone. *Science* 1995; 267:1796–1799.

[2] Yoshioka M, Yoshida Y, Inoue S, Lambrechts P, Vanherle G, Nomura Y,Okazaki M, Shintani H, Van Meerbeek B. Adhesion/Decalcification mechanisms of acid interactions with human hard tissues. *J Biomed Mater Res* 2002; 59:56–62.

[3] Penel G, Delfosse C, Descamps M, Leroy G. Composition of bone and apatitic biomaterials as revealed by intravital raman microspectrometry. *Bon*e 2005; 36:893–901.

[4] Pasteris JD, Wopenka B, Freeman JJ, Rogers K, Valsami-Jones E, Van der Houwen JAM, Silva MJ. Lack of OH in nanocrystalline apatite as a function of degree of atomic order: implications for bone and biomaterials. *Biomaterials* 2004; 25:229–238.

[5] Dorozhkin SV, Epple M. Biological and medical significance of calciumphosphates. Angew Chem Int Ed 2002; 41:3130–3146.

[6] Nancollas GH, Tang R, Phipps RJ, Henneman Z, Gulds S, Wu W, Mangood A, Russell RGG, Ebetino FH. Novel insights into actions of bisphosphonates on bone: differences in interactions with hydroxyapatite. *Bone* 2006;38: 617–627.

[7] Lin JH. Bisphosphonates: a review of their pharmacokinetic properties. *Bone* 1996; 18:75–85.

[8] Hoskin PJ. Bisphosphonates and radiation therapy for palliation of metastatic bone disease. Cancer Treat Rev 2003; 29:321–327.

[9] Zeevaart JR, Jansen DR, Botelho MF, Abrunhosa A, Gomes C, Metello L, Kolar ZI, Krijger G, Louw WKA, Dormehl IC. Comparison of the predicted in vivo behaviour of the Sn(II)–APDDMP Complex and the results as studied in a rodent model. *J Inorg Biochem* 2004; 98:1521–1530.

[10] Ogawa K, Mukai T, Arano Y, Otaka A, Ueda M, Uehara T, Magata Y, Hashimoto K, Saji H. Rhenium-186-monoaminemonoamidedithiol-conjugated bisphosphonate derivatives for bone palliation. *Nucl Med Biol* 2006; 33:513–520.

[11] Lewington VJ. Cancer therapy using bone-seeking isotopes. *Phys Med Biol* 1996; 41:2027–2042.

[12] Papapoulos SE. Bisphosphonate actions: physical chemistry revisited. *Bone* 2006; 38:613–616.

[13] Fleisch H. Bisphosphonates: mechanisms of action*. Endocr Rev*1998; 19:80–100.

[14] Rogers MJ, Gordon S, Benford HL, Coxon FP, Luckman SP, Monkkonen J, Frith JC. Cellular and molecular mechanisms of action of bisphosphonates. *Skelet Complic Malign, Suppl Cancer* 2000;88:2961–2978.

[15] Corbridge DEC. Phosphorus: *An Outline of its Chemistry, Biochemistry and Technology.* Amsterdam: Elsevier Scientific; 1990 (4[10] Studies in Inorganic Chemistry).

[16] Libson K, Deutch E, Barnett BL. Structural characterisation of a 99Tc–diphosphonate complex. Implications for the chemistry of 99mTc skeletal imaging agents. *J Am Chem Soc* 1980; 102:2476–2478.

[17] Penel G, Leroy G, Rey C, Sombret B, Huvenne JP, Bres E. Infrared and Raman microspectrometry study of fluor-, fluorhydroxy and hydroxy-apatite powders. *J Mater Sci, Mater Med* 1997; 8:271–276.

[18] Van Haverbeke L, Desseyn HO, Herman MA. Vibrational Spectra of mono- and polymethylene diphosphonic acids. *B Soc Chim Belg* 1972; 81:547–554.

[19] Mikelsons MV, Pinkerton TC. Raman spectroscopic evidence for Tc–Oxocores in Tc–HEDP complexes. Appl Radiat Isotopes 1987; 38:569–570.

[20] Myund LA, Bus'ko EA, Smirnova NI, Terekhin SN, Dyatlova NM, Burkov KA. Raman spectroscopy studies on the acid–base equilibria in 1-hydroxyethyl-1,1-diphosphonic acid solutions. *Vestn Lenin U Fiz Kh -Seriya* 4 1987; 3:48–53.

[21] Myund LA, Bus'ko EA, Terekhin SN, Burkov KA. Spectroscopic investigation of the deprotonation processes of 1-hydroxyethylidene-1,1-diphosphonic acid. *Vestn Lenin U Fiz Kh - Seriya* 4 1990; 1:33–37.

[22] Myund LA, Bus'ko EA, Terekhin SN, Burkov KA. Investigation of complexing Zn(II) with hydroxyethane diphosphonic acid in aqueous solution by Raman spectroscopy. *J Appl Spectrosc-Russian Ed* 1989; 50:416–420.

[23] Matveeva AG, Pasechnik MP, Petrovskii PV, Matveev SV, Pisareva SA. Amino-substituted gem–diphosphonic acids: dissociation mechanism and the structure of species in aqueous solutions. *Russ Chem, B* 2000;49:1045–1058.

[24] Bus'ko EA, Myund LA, Terekhin SN, Burkov KA, Dyatlova NM, Volkova NA. State of hydroxyethylidenediphosphonic acid in aqeous solutions. *ZhNeorg Khim* 1988 ;33:603–607.

[25] Hein LE, Grassi RL, Roldan EJA, Gregori D, Varela ME, Piccinni EP.Morphological studies of hydroxyapatite crystals exposed to disodium pamidronate. *Medicina* 1997; 57(Supplement 1):10–16.

[26] Aminzadeh A. Fluoresence bands in the FT-Raman spectra of somecalcium minerals. *Spectrochim Acta*, A 1997; 53:693–697.

[27] Uchtman VA. Structural investigation of calcium binding molecules. II.The crystal and molecular structures of calcium dihydrogen ethane-1-hydroxy-1,1-diphosphonate dihydrate, CaC(CH3)(OH)(PO3H)2.2H2O;implications for polynuclear complex formation. *J Phys Chem* 1972; 76:1304–1310.

[28] Wada H, Fernando Q. Interaction of methanehydroxyphosphonic acid and ethane-1,1-diphosphonic acid with alkali and alkaline earth metal ions. *Anal Chem* 1972; 44:1640–1643.

[29] Grabenstetter RJ, Cilley WA. Polynuclear complex formation in solutions of calcium ion ands ethane-1-hydroxy-1,1-diphosphonic acid. I. Complexometric and PH titrations. *J Phys Chem* 1971; 75:676–682.

[30] Wiers BH. Precipitation boundaries in calcium–pyrophosphate andcalcium–ethane-1-hydroxy-1,1-diphosphonate systems. *Inorg Chem1971*; 10:2581–2584.

[31] Penel G, Leroy G, Bres E. New preparation method of bone samples forRaman microspectrometry. *Appl Spectrosc* 1998; 52:312–313.

[32] SMART (Version 5.054), SAINT (Version 6.45), SADABS (Version 2.10) and SHELXTS/SHELXTL (Version 6.12). Bruker AXS Inc., Madison,Wisconsin, USA. 2001.

[33] SHELXS-97 and SHELXL-97. Sheldrick, GM University of Göttingen,Germany; 1997.

[34] Faruggia LJ. ORTEP-3 for Windows—a version of ORTEP-III with a graphical user interface (GUI). *J Appl Crystallogr* 1997; 30:565.

[35] Mercury (Version 1.4.2). Cambridge Crystallographic Data Centre. URL: http://www.ccdc.cam.ac.uk; 2007.

[36] POV-Ray for Windows. (Version 3.6) Persistence of Vision Raytracer Pty.Ltd., Victoria, Australia. URL: http://www.povray.org; 2004.

[37] Gaussian03, Revision D.01. Frisch, MJ, Trucks, GW, Schlegel, HB,Scuseria, GE, Robb, MA, Cheeseman, JR, Montgomery, JA, Vreven, T,Kudin, KN, Burant, JC, Millam, JM, Iyengar, SS, Tomasi, J, Barone, V,Mennucci, B, Cossi, M, Scalmani, G, Rega, N, Petersson, GA, Nakatsuji,H, Hada, M, Ehara, M, Toyota, K, Fukuda, R, Hasegawa, J, Ishida, M,Nakajima, T, Honda, Y, Kitao, O, Nakai, H, Klene, M, Li, X, Knox, JE,Hratchian, HP, Cross, JB, Bakken, V, Adamo, C, Jaramillo, J, Gomperts, R,Stratmann, RE, Yazyev, O, Austin, AJ, Cammi, R, Pomelli, C, Ochterski,JW, Ayala, PY, Morokuma, K, Voth, GA, Salvador, P, Dannenberg, JJ, Zakrzewski, VG, Dapprich, S, Daniels, AD, Strain, MC, Farkas, O,Malick, DK, Rabuck, AD, Raghavachari, K, Foresman, JB, Ortiz, JV, Cui,Q, Baboul, AG, Clifford, S, Cioslowski, J, Stefanov, BB, Liu, G,Liashenko, A, Piskorz, P, Komamori, I,

Martin, RL, Fox, DJ, Keith, T, Al-Laham, MA, Peng, CY, Nanayakkara, A, Challacombe, M, Gill, PMW, Johnson, B, Chen, W, Wong, MW, Gonzalez, C, and Pople, JA; 2004.

[38] Scott AP, Radom L. Harmonic vibrational frequencies: an evaluation of Hartree–Fock, Møller–Plesset, quadratic configuration interaction, density functional theory, and semiempirical scale factors. *J Phys Chem* 1996; 100:16502–16513.

[39] Sahar ND, Hong S-I, Kohn DH. Micro- and nanostructural analyses of damage in bone. *Micron* 2005; 36:617–629.

[40] Lin-Vien D, Colthup NB, Fateley WG, Grasselli JG. *Organophosphorous compounds. The Handbook of Infrared and Raman Characteristic Frequencies of Organic Molecules*. London: Academic Press Limited;1991. p. 263–276.

[41] Popovic L, De Waal D, Boeyens JCA. Correlation between Raman wave numbers and P–O bond lengths in crystalline inorganic phosphates. *J Raman Spectrosc* 2005;36:2–11.

[42] Zeevaart JR, Jarvis NV, Cukrowski I, Jackson GE. Blood plasma modelling of the in vivo behaviour of bisphosphonate–metal ion complexes as radiopharmaceuticals. *S Afr J Chem* 1997; 50:189–194.

[43] Berezin KV, Nechaev VV, Krivokhizhina TV. Application of a method of linear scaling of frequencies in calculations of the normal vibrations of polyatomic molecules. *Mol Spectrosc* 2003; 94:398–401.

[44] Berezin KV, Nechaev VV. Comparison of theoretical methods and basis sets for *ab initio* and DFT calculations of the structure and frequencies of normal vibrations of polyatomic molecules. *J Appl Spectrosc* 2004; 71:164–172.

[45] Silvestre J-P, Dao NQ, Leroux Y. A survey of the behaviour of the hydroxy bisphosphonic function in crystallized acids, metallic salts and some related compounds. *Heteroatom Chem* 2001; 12:73–89.

[46] Fiquet G, Richet P, Montagnac G. High-temperature thermal expansion of lime, periclase, corundum and spinel. *Phys Chem Miner* 1999; 27:103–111.

[47] Casciani FS, Condrate Sr RA. The infrared and Raman spectra of several calcium hydrogen phosphates. *Proc Int Congr Phosphorous Compds* 1980; 2: 175–190.